Vane–Probe Interactions in Transonic Flows

Article *in* Journal of Turbomachinery · December 2022

DOI: 10.1115/1.4056578

CITATIONS
2

READS
57

5 authors, including:

Antonino Federico Maria Torre
von Karman Institute for Fluid Dynamics
8 PUBLICATIONS **10** CITATIONS
SEE PROFILE

Marios Patinios
General Electric
25 PUBLICATIONS **109** CITATIONS
SEE PROFILE

Gustavo Lopes
von Karman Institute for Fluid Dynamics
12 PUBLICATIONS **5** CITATIONS
SEE PROFILE

Sergio Lavagnoli
von Karman Institute for Fluid Dynamics
81 PUBLICATIONS **508** CITATIONS
SEE PROFILE

Vane–Probe Interactions in Transonic Flows

Antonino Federico Maria Torre[1]
Turbomachinery and Propulsion Department,
von Karman Institute for Fluid Dynamics,
Rhode Saint-Genèse 1640, Belgium
e-mail: antonino.torre@vki.ac.be

Marios Patinios
Turbomachinery and Propulsion Department,
von Karman Institute for Fluid Dynamics,
Rhode Saint-Genèse 1640, Belgium
e-mail: marios.patinios@ge.com

Gustavo Lopes
Turbomachinery and Propulsion Department,
von Karman Institute for Fluid Dynamics,
Rhode Saint-Genèse 1640, Belgium
e-mail: gustavo.lopes@vki.ac.be

Loris Simonassi
Turbomachinery and Propulsion Department,
von Karman Institute for Fluid Dynamics,
Rhode Saint-Genèse 1640, Belgium
e-mail: loris.simonassi@vki.ac.be

Sergio Lavagnoli
Turbomachinery and Propulsion Department,
von Karman Institute for Fluid Dynamics,
Rhode Saint-Genèse 1640, Belgium
e-mail: sergio.lavagnoli@vki.ac.be

In this article, a numerical investigation of the effect of a miniaturized five-hole probe downstream of a transonic low-pressure turbine vane row is presented. First, a numerical calibration of the probe was performed in uniform flow conditions, as is the case for any traditional calibration, for a wide range of Mach number, yaw angle, and pitch angle conditions. The effect of the probe on the general flow field throughout the turbine vane segments was then evaluated by performing a comparison between a setup with vanes only (no probe) and with vanes and probes. It was found that, as the probe traverses downstream the vane, the probe impact on the vane isentropic Mach number depends on the probe circumferential position. The highest impact was observed when the probe is located at the upper mid-passage ($\theta = 0.5$), consisting of a relatively small reduction of the isentropic Mach number on the vane suction side of just 0.02. To assess the accuracy of the quantities "measured" by the probe, the probe-determined flow field was compared to the flow field of the vanes-only setup. A nonnegligible modification of the probe-determined local distributions of Mach number, yaw angle, and pitch angle is revealed with respect to the undisturbed flow. Further investigation involving stagnation point tracking showed that the artificial high circumferential variation of the yaw angle is not caused by a modification of the vane outlet flow angle, but is induced by nonuniform flow conditions downstream of the vanes. With knowledge of the above, a two-step correction is used to account for the effects of the nonuniformity of the flow, and its impact is evaluated on 2D and 3D flow regions. A significative effect of the correction was found on the probe-determined yaw angle, in which the difference from the vanes-only data was reduced to below 1 deg, except near the endwalls where larger discrepancies remain due to probe–endwall interactions. A shortfall of the correction was instead observed on the probe-determined Mach numbers. Finally, the pitch-wise averaged quantities were evaluated. It was observed that the highest differences between probe-determined and undisturbed data occur where radial gradients of total pressure are stronger and that the two-step correction had almost negligible impact on the pitch-wise averaged quantities.
[DOI: 10.1115/1.4056578]

Keywords: probe blockage, vane–probe interaction, five-hole probe, transonic vane, impact on measurements, measurement corrections, computational fluid dynamics (CFD), measurement techniques, turbine blade and measurement advancements

1 Introduction

Multi-hole probes are often used in many experimental fields as a robust and cost-effective tool to measure important aerodynamic quantities. One such field is turbomachinery, where multi-hole probes are widely used due to easiness of implementation and their compact design, which allows for employment even in the smallest of spaces. The immersion of the probe in the flow generates a local blockage [1] and induces perturbations that fundamentally change the flow field and affect the aerodynamics of the test article [2]. These effects become even more significant when the Mach number approaches transonic values [3].

The interaction between airfoils and directional probes has a considerable impact on the measured flow quantities. This interaction was numerically studied by Aschenbruck et al. [4] on the last stage of an axial turbine and Sanders et al. [5] on a high-speed compressor test case. Both studies showed that the data retrieved by the modeled probe differed from the numerical results obtained from a "clean" test case without the probe.

Boerner et al. [3] compared the experimental measurements of pneumatic five-hole probe with particle image velocimetry (PIV) measurements downstream of a turbine linear cascade. In this study, the authors investigated the effect of the Mach number on the interaction between five-hole probe measurements. It was shown that when approaching sonic conditions, the measured Mach number fails in the proximity of the wake.

Hoenen et al. [6] studied the effect of the pressure gradients on the pneumatic probe measurements using a five-hole probe downstream of a symmetric NACA-65 profile located in front of a nozzle. Tests were conducted at two different Mach numbers (0.3 and 0.5) and at several axial distances between airfoil trailing edge and probe. The probe data were compared against the data from a split film probe, which were used as the reference data. The trailing edge gradients were shown to have a significant impact on the probe measurements of Mach number and flow angles. The authors showed that a correction applied to account for the spatial distance of the pressure taps could reduce the error in the flow angle measurements. Nonetheless, an error of two deg persisted after the correction, which was invariant with distance between the airfoil trailing edge and the probe head. The authors attributed this error to the blockage of the probe stem.

The inaccuracies highlighted by the probes in the presence of pressure gradients are attributed to the fact that probe calibration is generally performed in the uniform flow [7]. Total pressure gradients impinging on the multi-hole probe generate a pressure difference between pressure taps, which, when using a uniform probe calibration, is erroneously attributed to an incidence effect. Correction procedures have been developed to overcome these errors [8,9]. The validation of this procedure is, however, often performed on 2D flow regions.

[1]Correponding author.
Manuscript received July 19, 2022; final manuscript received December 18, 2022; published online January 9, 2023. Tech. Editor: David G. Bogard.

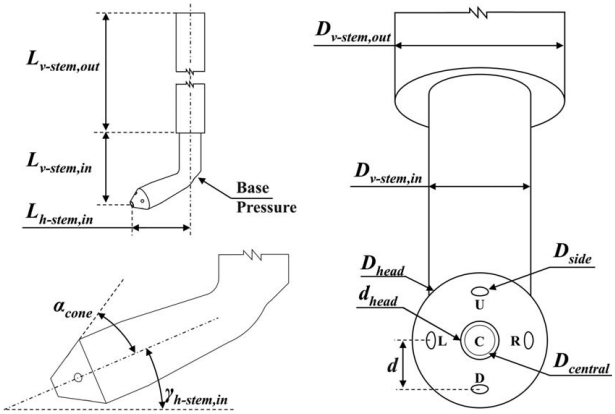

Fig. 1 Five-hole probe geometry and key parameters

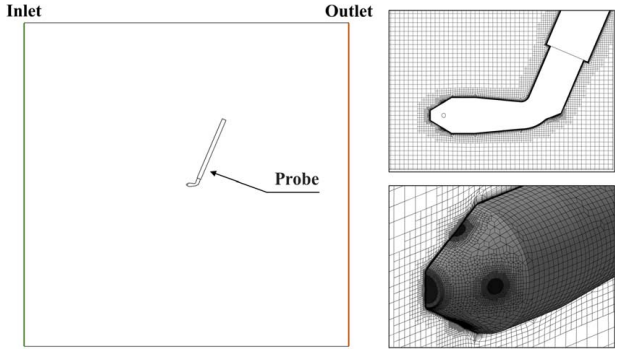

Fig. 2 Probe calibration setup and mesh lookup

In this article, the effect of a miniaturized five-hole probe on the flow field downstream of a transonic low-pressure turbine vane row sector is investigated using numerical simulations. The underlying physical effects of the interaction between vane and probe are analyzed on the freestream. A thorough analysis of the probe-determined data is undertaken to identify the sources of differences from the results of the undisturbed field. Finally, the fidelity of the probe-determined data in the 2D and 3D flow regions is evaluated.

2 Numerical Calibration

2.1 Probe Geometry. Figure 1 shows the geometry of the probe that was used in this study. Key dimensions are marked in the figure, and their respective values are reported in Table 1. The probe is of an "L" shape and consists of an outer vertical stem with diameter, $D_{\text{v-stem,out}} = 4$ mm and length, $L_{\text{stem,out}} = 63.6$ mm, an inner vertical stem with diameter, $D_{\text{v-stem,in}} = 2.4$ mm and length, $L_{\text{v-stem,in}} = 10$ mm, and a horizontal stem (with a conical measurement head) of reducing diameter and axial length, $L_{\text{h-stem,in}} = 9.5$ mm. The horizontal stem is set with a pre-pitch angle relative to the axial direction, $\gamma_{\text{h-stem}} = 23$ deg to follow the mean pitch angle of the flow at the measurement location so as to limit the calibration range.

The conical head of the probe has a cone angle, $\alpha_{\text{cone}} = 31$ deg with a major diameter, $D_{\text{head}} = 3.2$ mm and a minor diameter, $d_{\text{head}} = 0.9$ mm. The head also features five pressure taps, one at the tip of the cone, referred to as the central hole (C), and four side holes, drilled normal to the surface of the cone, and referred to as the up (U), down (D), left (L), and right (R) holes. For simplification of the numerical mesh, the pressure taps are modeled as patches with circular shapes. The diameter of the central hole patch is 0.71 mm, whereas the diameter of the side hole patches is 0.4 mm.

Table 1 Probe key parameters values

Parameter	Dimension (mm)
D	0.9
d_{head}	3.2
D_{central}	0.71
D_{head}	3.2
D_{side}	0.4
$D_{\text{v-stem,in}}$	2.4
$D_{\text{v-stem,out}}$	4
$L_{\text{h-stem,in}}$	9.5
$L_{\text{v-stem,in}}$	10
$L_{\text{v-stem,out}}$	63.6

The probe also features an additional tap, also modeled as a patch, with the same diameter as the side taps. This tap is located near the rear end of the vertical stem and is referred to as the base pressure tap. As the probe measurements are performed in a flow field of highly subsonic Mach numbers, the addition of the base pressure tap enables for calibration with a higher Mach number sensitivity and thus less measurement error [10].

2.2 Numerical Setup and Mesh for Calibration. The numerical calibration [11,12] of the probe is performed using the commercial software NUMECA FINEOPEN 8.2. To obtain the calibration coefficients, steady Reynolds-averaged Navier–Stokes (RANS) simulations were performed using the k-ω shear stress transport (SST) turbulence model [13]. The spatial discretization employed is a second-order central scheme. The fluid domain consists of a cubic volume containing the probe, as shown in Fig. 2. The volume top, bottom, and side surfaces are set as periodic boundaries, and the size of the cube is 100 times the probe diameter.

The probe central hole is centered inside the volume, and the probe head axis is normal to the domain inlet. The orientation of the probe is not changed throughout the calibration. Various flow yaw and pitch angles are instead achieved by varying the inlet boundary conditions. This calibration procedure was exceptionally convenient because it allowed the use of a single mesh for covering the complete calibration matrix.

The unstructured hexahedral mesh was generated using NUMECA's HEXPRESS™ 8.2 mesh generator. Higher refinement is done close to the probe geometry with further refinement in the proximity of the hole patches, as shown in Fig. 2 (right). Viscous layers with a minimum thickness of 1 μm have been applied over the solid surfaces and hole patches, achieving global $y+$ below unity. The mesh of the calibration setup is constituted by approximately three million cells.

A mesh sensitivity analysis was performed against coarser (about 1.8 million cells) and finer (about 12.8 million cells) grids. To evaluate mesh sensitivity, the average static pressure from the four side hole patches was compared across all different grids for an inlet flow with $\alpha = 15$ deg, $\gamma = 15$ deg, and $M = 0.95$.

Between the baseline and refined grids, the average pressure difference between the hole patches is 0.2% of the inlet total pressure, while the difference between the coarse and refined grids is 0.33% of the inlet total pressure. Based on this, the baseline grid was chosen as it allows to obtain accurate results with a 25% lower computational cost in comparison to the refined mesh.

2.3 Calibration Procedure. The angle and conditions of the flow measured by the probe (Fig. 3) are obtained by associating the pressure readings of the probe taps with values of yaw, pitch, Mach number and pressures by means of coefficients retrieved through calibration. Experimental calibrations are typically performed in a uniform and well-characterized jet delivered by a nozzle [14,15]. Following the same way, a uniform inlet flow was

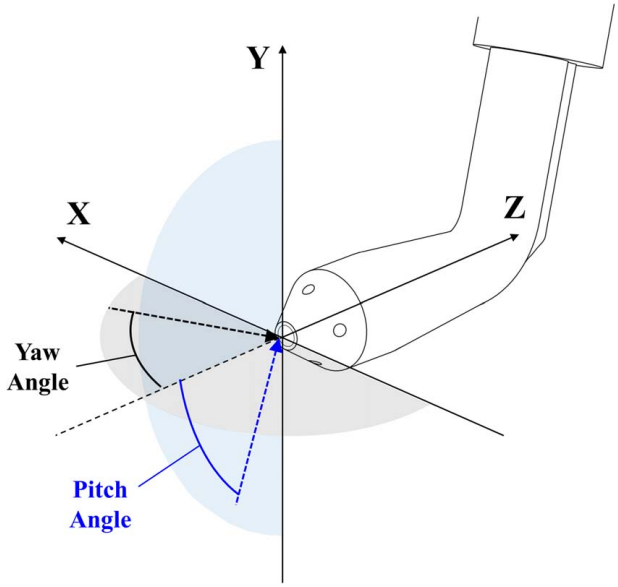

Fig. 3 Flow angles with respect to the probe system of reference

also used for the numerical calibration performed in this study, the conditions (α, γ, M, and P_t) of which are computed by a mass flow average at the inlet of the domain.

The calibration coefficients are calculated by using the definitions adopted by Passmann et al. [3] as follows:

$$K_{\text{yaw}} = \frac{P_L - P_R}{P_C - P_{\text{ave}}} \tag{1}$$

$$K_{\text{pitch}} = \frac{P_D - P_U}{P_C - P_{\text{ave}}} \tag{2}$$

$$K_{\text{mach}} = \left(\frac{2}{\gamma - 1} \left[\left(\frac{P_{\text{ave}}}{P_C} \right)^{-\frac{\gamma-1}{\gamma}} - 1 \right] \right)^{1/2} \tag{3}$$

$$K_{\text{tot}} = \frac{P_C - P_{\text{tot}}}{P_C - P_{\text{ave}}} \tag{4}$$

where

$$P_{\text{ave}} = \frac{P_U + P_D + P_L + P_R}{4} \tag{5}$$

In the aforementioned definitions, subscripts C, U, D, L, and R correspond to the various taps of the probe, as shown in Fig. 1. The value of static pressure P used for each of the taps is the value of the average static pressure on the respective hole patch. As an alternative to using the average pressure in Eq. (5), the base pressure (referred as P_{BP}) can be used in the aforementioned definitions to calculate the calibration coefficients so that a higher Mach number sensitivity can be achieved.

The calibration was performed for seven pitch angles, from −15 deg to +15 deg in steps of 5 deg, and four yaw angles from 0 deg to +15 deg in steps of 5 deg. To limit the number of simulations, the calibration was performed only on positive yaw angles and was assumed symmetric for the negative yaw angles.

The probe was also calibrated for five Mach numbers (0.55, 0.70, 0.8, 0.9, and 0.95), from subsonic to transonic conditions. The flow Mach number was set by maintaining a constant inlet pressure and varying the outlet static pressure, thus changing the total-to-static pressure ratio that determines the Mach number. In total, 140 conditions have been used to perform the numerical calibration.

The accurate measurement of the total pressure depends on the value of the stagnation pressure measured by the central hole of the probe. In retrieving the stagnation pressure, the level of turbulence plays a major role. Issa [16] showed analytically that on stagnation flows, a rise in total pressure occurs along the streamline due to the mechanical energy redistribution through viscous shear stresses. Issa concluded that this effect is proportional to the viscosity and therefore occurs with higher intensity in turbulent flows rather than laminar. In the study by Norris [17], it was shown that the use of turbulence eddy viscosity models induces a spurious growth of the total pressure at the stagnation point as the viscosity decreases along the streamline. As Williams et al. [18] pointed out, these spurious effects rising from eddy viscosity modeling are an accurate solution to the governing equations. With their numerical results, they showed that in a massively separated flow, the total pressure presents a physically spurious increase that occurs for different grid refinements, solution convergences, and turbulence models. As mentioned earlier, the turbulence intensity level at which the numerical calibration is performed is of primary importance for obtaining the correct calibration coefficients to be later employed in the measurements. The five-hole probe was therefore calibrated at the same turbulence conditions as the ones found downstream of the vane row. These conditions were identified through a separate computational fluid dynamics simulation, discussed later in the article, which included the vanes.

Following the approach described by Main et al. [19], a calibration matrix of coefficients K_{yaw}, K_{pitch}, and K_{Mach} is generated at regular steps of α, γ, and M. The linear interpolation functions of α, γ, M, and K_{tot} have been created on the calibration grid of K_{yaw}, K_{pitch}, and K_{Mach}. During the measurements, flow pressures, angles, and Mach number are obtained from the interpolant functions by an indexed lookup using coordinates of K_{yaw}, K_{pitch}, and K_{Mach} measured by the probe.

Figure 4 (left) shows the characteristic total pressure coefficients at Mach number equal to 0.8 using P_{ave} and P_{BP}. Figure 4 (right) shows the variation of K_{Mach} with the freestream Mach number. Using P_{BP}, a much higher sensitivity of the Mach number coefficient on every calibration point can be seen, while using P_{ave} results in a flattening of the slope of curve when approaching the sonic condition, thus reducing the sensitivity to Mach number and increasing the error in the measurement.

Figure 5 shows the orthogonality maps of the calibrated probe when P_{ave} (left) and P_{BP} (right) are used. The orthogonality maps obtained using P_{ave} do not change with different Mach numbers. When P_{BP} is used, the maximum and minimum values of yaw and pitch angle coefficients decrease in absolute value, as the Mach number increases. The "shrinking" of the orthogonality map of Fig. 5 (right) occurs due to a reduction of the static pressure level during calibration that makes the denominator of Eqs. (1), (2), and (4) to increase. This effect implies an unfavorable reduction of pitch and yaw angle sensitivity. The measurements discussed in Sec. 4 will employ the traditional side holes pressure average (P_{ave}) and not the base pressure to compute the calibration coefficients. The average quantities are preferred for this study to not reduce the sensitivity to yaw and pitch angle coefficients; a choice justified by the fact that at the test Mach number of M ∼ 0.8, the curve of K_{Mach} versus Mach number in Fig. 4 (right) has still a positive slope.

3 Effects of Probe–Vane Interactions on Flow Field and Probe Measurements

3.1 Numerical Setup and Mesh. To investigate the effects of probe–vane interactions on the measurements of the five-hole probe, two numerical setups were simulated, one in which both the vanes and probes are present and one in which only the vanes are present, i.e., without probe.

Figure 6 shows the numerical setup for the case where both vanes and probe are present. This setup consists of two annular-sector domains, a stationary domain containing one vane passage and a

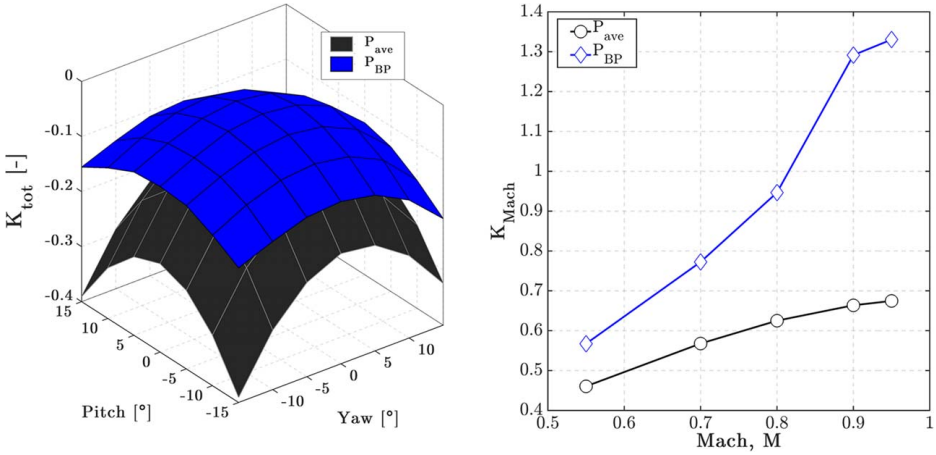

Fig. 4 K_{TOT} coefficients at M = 0.8 (left) and variation of Mach coefficient with Mach numbers at zero incidence (right) for P_{ave} and P_{BP}

rotating domain containing the probe. The probe domain is extended circumferentially for eight vane passages to reduce the periodic propagation of the potential field of the probe, thus resulting in a periodicity between the stationary and the rotating domains equal to 8:1. The inlet of the domain was set to 1.75 axial chords upstream of the vane leading edge where inlet boundary distributions of total pressure, temperature, and flow angles are known. The two domains are separated by a stator–rotor interface, located approximately halfway between the vane trailing edge and plane 2 where the probe measurements are performed.

The probe is located at half axial vane-chord downstream of the vane trailing edge and is traversed in the circumferential direction by imposing a speed of less than 10 rpm to the rotating domain, where the probe is contained. This speed was chosen such as to be representative of the traversing system to be used in the upcoming experimental campaign.

The circumferential traverses are performed at 14 different span-wise locations: one location at mid-span to investigate the effect of the vane–probe interactions in the 2D flow region, and six locations near the hub and seven locations near the shroud to investigate the vane–probe interactions in the 3D flow region. The span-wise resolution ranges from 1% to 5% of the span, being finer near the end-walls and coarser away from them.

The test case where only the vanes are present (or the no-probe case) provides the "undisturbed" flow field through the vane row and is used as the reference case to which the results obtained in the vane and probe setup are compared. The setup of the vanes-only case is identical to the one where both vanes and probes are present with the only difference being that the rotating domain is just a fluid volume with no probe included.

The simulation boundary conditions are set such as to obtain for the undisturbed flow field the aerodynamic conditions reported in Table 2.

Figure 7 shows the mesh of the vane and probe domains. The vane domain consists of 1.6 million cells, while the rotating domain consists of approximately nine million elements. Mesh refinement on the probe is performed in such a way to create consistency with the mesh characteristics used for the numerical calibration setup. Boundary layers are resolved on both domains reaching a $y+<1$.

The numerical simulations have been performed using the commercial software NUMECA FINEOPEN 8.2 employing the *K-ω SST* turbulence model and second-order central scheme. The unsteady solutions have been computed using the nonlinear harmonic approach first introduced by He and Ning [20]. This method is particularly advantageous from a computational effort perspective as it allows for a tenfold reduction in the time to achieve a converged solution with respect to the phase-lag solution, while producing similar results [21]. The harmonic solution is then reconstructed in time to 30 circumferential probe positions in one vane passage, resulting in a pitch-wise resolution at midspan of 1.5 times the vane trailing edge.

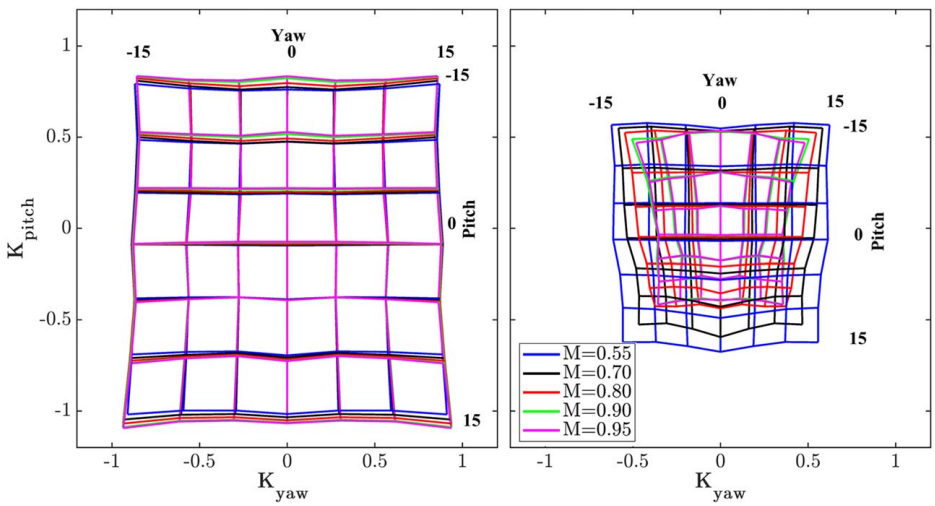

Fig. 5 Orthogonality maps for P_{ave}-based coefficients (left) and P_{BP}-based coefficients (right)

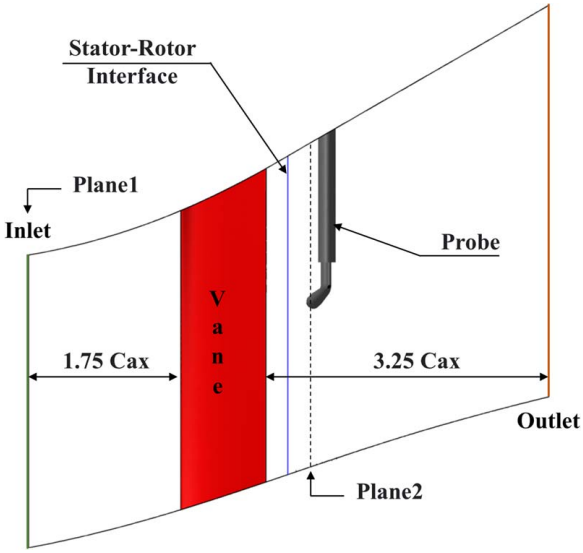

Fig. 6 Probe disturbance setup

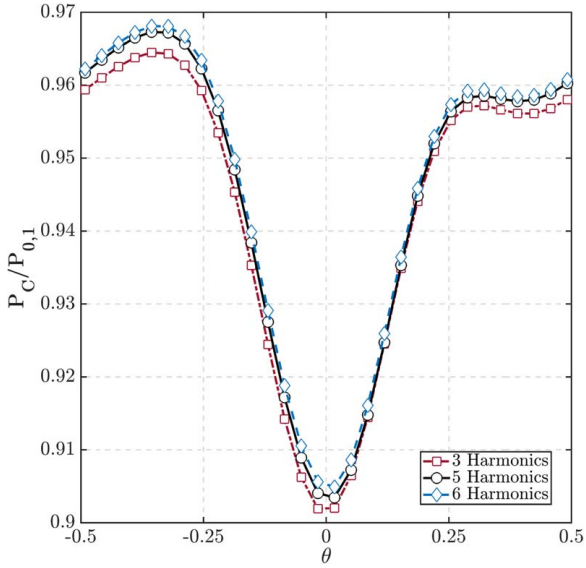

Fig. 8 Sensitivity analysis on the number of harmonics

Table 2 Vane aerodynamics parameters at undisturbed flow conditions

Parameter	Value
Reynolds number (vane outlet and C_{ax}), Re	1.67×10^5
Vane exit Mach number, M	0.8
Vane pressure ratio, $P_{t,in}/P_{out}$	1.48
Turbine mass flowrate, $\dot{m}$ (kg/s)	10.5

The level of accuracy of the solution can be controlled through the number of harmonics propagated between the two domains. A sensitivity analysis on the number of harmonics was performed for the probe traversing at midspan. Figure 8 shows the pitch-wise distribution of the pressure of the central tap for three different selected harmonics. Minor differences are observed between five and six harmonics, resulting in a difference in the pitch-wise average of just 0.1% of the inlet total pressure. Using three harmonics would result instead in a difference in the pitch-wise average value with respect to the six harmonics case of 0.3%. Based on the aforementioned facts, the perturbation of five harmonics of the probe passing frequency has been used in this study, giving a good balance between computational time and accuracy of the results.

3.2 Effect on the Flow Field. Figure 9(*a*) shows the static pressure distribution through the vane and probe domains on an axial-tangential plane at midspan, covering four vane passages in the tangential direction. For these results, the probe head was located at mid-span and at mid-pitch between airfoils 0 and 1.

A high static pressure region can be seen on the front part of the probe as a result of the stagnating flow on the head of the probe. A low-pressure region can also be found on the back of the probe due to the accelerating flow around the head of the probe. These high- and low-pressure regions affect the flow through the vane passages by altering the static pressure conditions at the outlet of each passage. Treating each passage as a nozzle, any change in the outlet static pressure results in a change of the pressure ratio across the nozzle, which in turn causes a change in the mass flow passing through it and a subsequent change of the static pressure distribution in the passages.

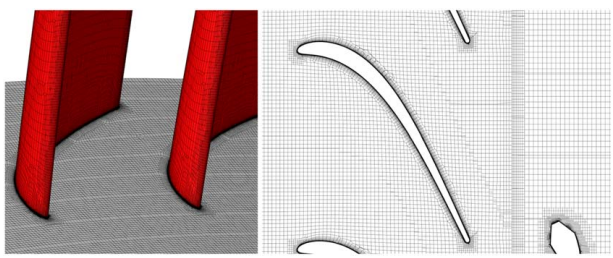

Fig. 7 Probe–vane mesh

The high static pressure at the front of the probe decreases the nozzle pressure ratio, thus decelerating the flow; this effect occurs in the flow of the two passages around the central vane 0, between vanes −1 and 1. On the contrary, the low static pressure around the probe decreases the nozzle pressure ratio, thus accelerating the flow; an effect is seen in the lower passages, between vanes −1 and −3.

The influence of the probe on the isentropic Mach number distribution on the surface of all eight vanes in the domain is shown in Fig. 9(*b*). In this figure, the isentropic Mach number distribution for the "clean" configuration without probe (referred to as "undisturbed" in the figure) is also shown.

In general, the influence of the probe on the Mach number distribution around the vanes is limited to the suction side only (negligible effect on the pressure side distributions) and varies between the different vanes.

Focusing on the suction side distributions, an acceleration of the flow relative to the undisturbed case can be seen for vanes −2 and −3 and a deceleration for vanes −1 to 1. This is as a result of the acceleration and deceleration of the flow in the respective passages due to the effect of the high- and low-pressure regions of the probe on the flow through the nozzles. The influence of the probe on the flow field diminishes with circumferential distance away from the probe, and therefore, the Mach number distributions for vanes beyond vane −3 and 1 are virtually identical to the undisturbed case.

A similar effect is observed when the probe is almost fully immersed. In this case, however, a much bigger probe impact is observed due to the larger blockage as a result of both larger penetration and higher Mach numbers at the hub.

Figure 10 shows the isentropic Mach number distribution on the surface of the central vane at midspan, for different circumferential positions of the probe when the probe head is located at midspan. The undisturbed vane isentropic Mach number distribution is also shown in the figure for comparison. The presence of the probe results in a reduction of the isentropic Mach number distribution, which is particularly evident on the rear of the suction side of the vane. The highest reduction in Mach number ($\Delta M_{max} = 0.02$),

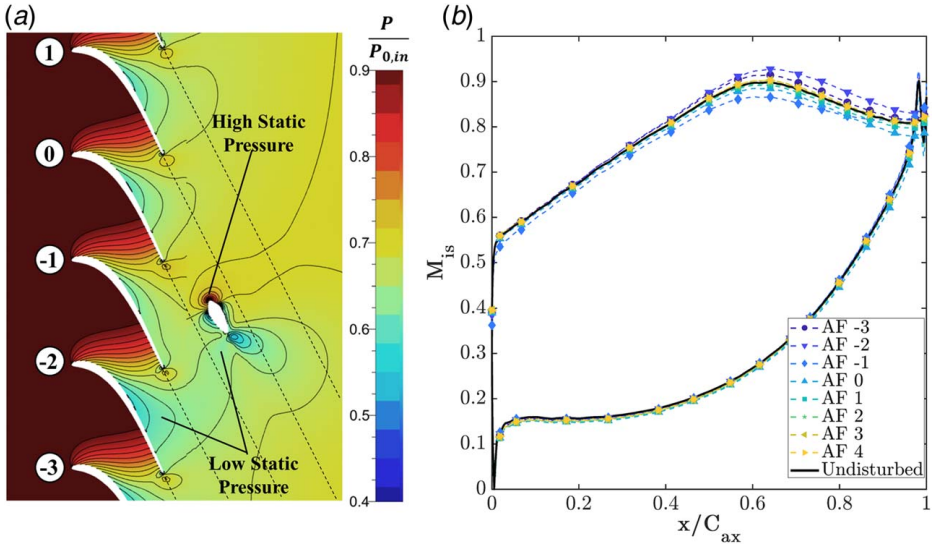

Fig. 9 (*a*) Static pressure contours across the vane row at midspan and (*b*) isentropic Mach number distribution on the airfoils at 50% of the span. Results for probe head located at mid-passage and probe inserted to 50% of the flow path span.

and hence the strongest influence of the probe, is shown for the case where the probe is at $\theta = +0.5$; the location at which the high static pressure in front of the probe head interacts with the passage formed between the suction side of the central vane and the pressure side of the adjacent vane. Interestingly, when the probe is in the negative pitch position ($\theta < 0$), there is almost no impact on the Mach number distribution on the vane. The aforementioned observations are in agreement with the experimental findings of Truckenmüller and Stetter [2] who tested the intrusiveness of pneumatic probes downstream of transonic guide vanes. Similarly, to what was shown in Fig. 10, Truckenmüller and Stetter reported no influence on the blade loading when the probe is in the negative pitch position and the highest reduction of dynamic pressure when the probe is in proximity of the upper mid-passage ($\theta = 0.5$).

3.3 Effect on the Probe Measurements in the 2D Region. Figure 11 shows the pitch-wise distributions of (*a*) normalized total pressure, (*b*) Mach number, (*c*) yaw angle, and (*d*) pitch angles in plane 2 at 50% span. The distributions of the reference test case (solid lines) and raw probe measurements (black circle symbols) are included in all of the plots.

The probe-determined nondimensional total pressure distribution (Fig. 11(*a*)) is in excellent agreement with the undisturbed values over most of the vane pitch, except in the wake where the total pressure is underestimated by 0.3% of the inlet total pressure.

The Mach number distribution (Fig. 11(*b*)) is, however, not very accurately retrieved by the probe. The probe-determined data show an overshoot of the Mach number on the edges of the wake and a strong Mach number reduction with respect to the vanes-only case in the wake. The same trend is shown from the comparison between five-hole probe and PIV measurements presented by Boerner et al. [3]. These discrepancies are mainly due to the probe not being able to correctly retrieve the static pressure distribution in the flow field as a result of the shortfallings of the uniform calibration, which are discussed in more detail later on in this section.

Figure 11(*c*) shows the pitch-wise distribution of the yaw angles of the vanes-only case and the probe-retrieved data. Data obtained from the vanes-only case show a low pitch-wise variation about the mean value of less than ±0.5 deg. On the contrary, the probe-determined data show a strong variation in the pitch-wise direction resulting in overestimation and underestimation of the flow angle with respect to the mean value of ±2 deg. It is noted that the highest variations are observed close to the strongest total pressure gradients.

The pitch angle distributions are shown in Fig. 11(*d*). For the vanes-only case, the pitch angle varies of ±1 deg about the mean value. The probe-determined data show that the pitch angle is underestimated over the majority of the vane passage due to a reduction of the pitch angle of the freestream in proximity of the probe head. This effect is caused by the prominent blockage of the probe stem that deviates the flow downward. The biggest difference between probe-determined data and vanes-only flow field is of 4 deg at $\theta = -0.05$ with respect to the vanes-only case.

To explain the large discrepancies in the flow angles between the undisturbed and probe-determined distributions, a stagnation point analysis was performed on the probe head. In this analysis, maximum and minimum yaw and pitch angles of the probe-

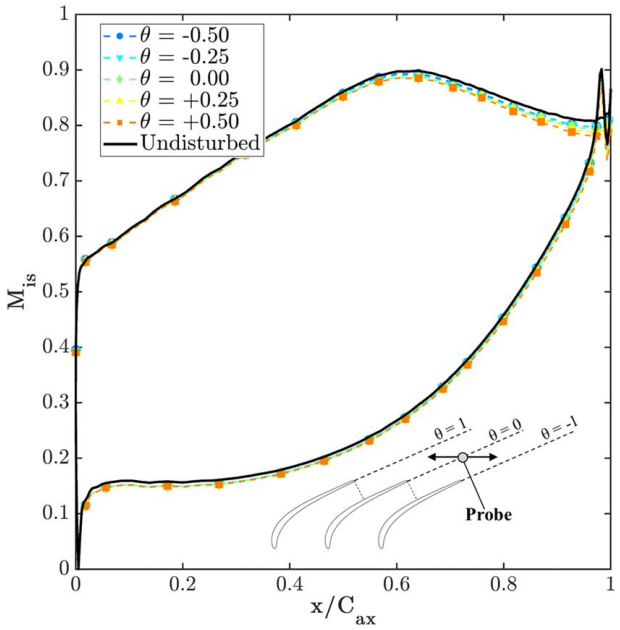

Fig. 10 Isentropic Mach number distribution on the central airfoil for different circumferential positions of the probe. Probe inserted to 50% of the flow path span.

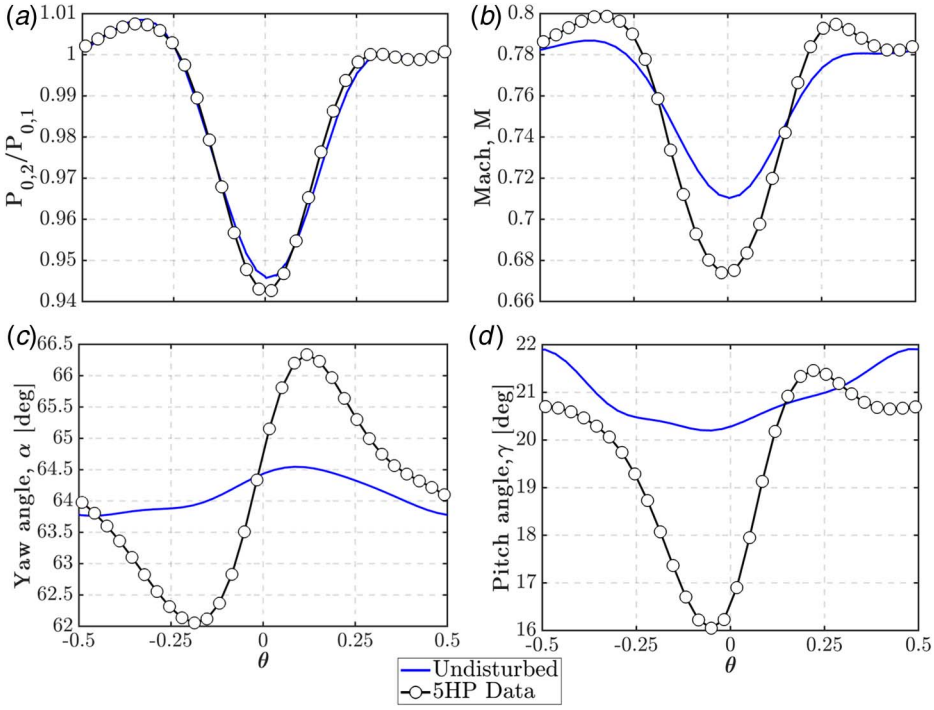

Fig. 11 Midspan pitch-wise distributions of (*a*) normalized total pressure, (*b*) Mach number, (*c*) yaw angle, and (*d*) pitch angle of the vanes-only case and measurement performed with the five-hole probe

determined distributions in the vane and probe setup (black line in Figs. 11(*c*) and 11(*d*)) were imposed as boundary conditions to the calibration setup and the resulting location of the stagnation points on the probe head were recorded. By using the positions of these stagnation points, an area was able to be identified, signifying the region in which all of the stagnation points generated in the vane and probe setup would have had to fall in if the probe were to be indeed measuring the real, undisturbed flow field.

Figure 12 indicates this region by a light blue-shaded rectangle. The locations of the stagnation points achieved during the traverse of the probe in the vane and probe setup are also indicated in the same figure by red circles. As it can be seen, all of the red circles are concentrated in a very small area and fall outside of the light blue-shaded region. This shows that the flow field measured by the probe has a much smaller yaw and pitch angle variation than the one actually determined by the probe.

Yaw and pitch angles are determined by five-hole probes based on differences in pressure between the left and right and top and bottom holes, which are then related to actual flow angles through calibration. These pressure differences are as a result of the pressure field generated around the probe when the flow impinges on the probe head. For the same flow angle, the pressure field will, however, be different in the case of a uniform pressure inlet calibration and in the case of a nonuniform pressure field such as the one experienced by the probe when positioned downstream of the vanes. Using a uniform calibration (like in this article and in most real application cases) for determining the flow angles in nonuniform flows results in an incorrect association of the pressure differences read by the probe and is what causes the error in the probe-determined angles shown in Fig. 11.

This phenomenon can be broken down into two causes: first the unavoidable distance between the side pressure taps (left to right or up to down), which exposes them in pressure gradients even at zero flow incidence, and second the transversal velocity component generated on the probe head when subjected to streamwise velocity (or total pressure) gradients [8].

A two-step correction to compensate for the errors caused by the aforementioned causes was presented by Ligrani et al. [8]. The first step accounts for the local displacement of the side taps on the probe head with respect to the central tap.

As shown in Fig. 13, measurements are taken when the probe central tap is at locations $k = 1, 2, 3 \ldots n$. The left and right taps are, respectively, located at $y(k) - d$ and $y(k) + d$, where d is the spatial distance between the central and side taps. As a result, during a complete traverse of the probe, the side taps evaluate the pressure at a different location than the central tap. Using the left tap as an example, this location is at $y(k) - d$. The value of pressure that the left tap would measure at the same location as the central tap can be estimated through linear interpolation between two adjacent points, $y(k) - d$ and $y(k+1) - d$. The same approach is used to estimate the values that would have been measured at the central tap position by the right tap. Following this approach, the values of pressures of every tap at $y(k)$ are now known and are used to evaluate the flow quantities. The procedure described earlier is used to correct for the spatial displacements of the taps in the y-direction and can be applied also in the z-direction.

The second step of the correction is used to compensate for the component of secondary transversal velocity rising when blunt bodies are subjected to gradients in the streamwise velocity component. The corrected velocity components are given by the following

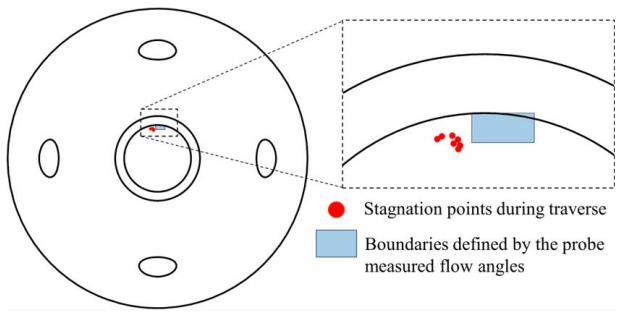

Fig. 12 Stagnation points on the probe head during the traverse and stagnation regions estimated from the probe measurements

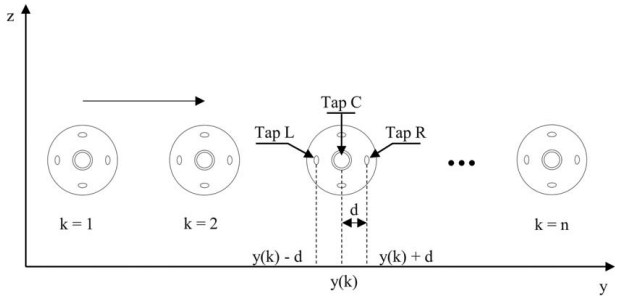

Fig. 13 Five-hole probe movement and port relative position respect to the central tap

formulas:

$$V_x = V_{x,u} + C\, dV_z/dx \tag{6}$$

$$V_y = V_{y,u} + C\, dV_z/dy \tag{7}$$

where $V_{x,u}$ and $V_{y,u}$ are the uncorrected components of tangential and radial velocities, respectively; V_x and V_y are the corrected components of tangential and radial velocities; V_z is the axial velocity component; and C is a coefficient dependent on the probe size. From the study by Ligrani et al. [8], the value of C equals 20% of the probe head diameter. A similar value (19%) was later confirmed by the work of Chernoray and Hjärne [9]. Both works employ five-hole probes with conical-shaped head operated in the low subsonic regime.

In the present work, the correction coefficient C was recomputed in the transonic regime, at which the probe is operated, and for Mach number M = 0.8 was found to be equal to 25.1% of the probe diameter. The procedure followed to obtain the correction coefficient is detailed in the Appendix.

For the purpose of this study, the two-step correction is performed only in the tangential direction as applying the correction in the radial direction was found to have negligible effects. Another reason for not applying the correction in the radial direction is that the radial interpolation would have caused the loss of information of the already few traversing points in the span-wise direction.

The final flow velocity is then computed accounting for the corrected tangential and radial velocity, and the measured axial velocity is expressed as follows:

$$V = \sqrt{V_x^2 + V_y^2 + V_z^2} \tag{8}$$

Ultimately, the Mach number can be computed as follows:

$$M = V/\sqrt{\gamma\, R\, T} \tag{9}$$

Figure 14 is a repeat of Fig. 11 with the addition of the distributions resulting from the application of the spatial displacement correction (green diamonds), the complete two-step correction with correction coefficient provided from literature, $C = 20\%$ of the probe diameter (purple triangles), and the complete two-step correction with correction coefficient recomputed at transonic Mach numbers, $C = 25.1\%$ of the probe diameter (red squares).

As shown in Fig. 14(*a*), the distributions of the probe-determined nondimensional total pressure with and without correction are identical, indicating that the effect of the correction is negligible on the measured total pressure value.

The Mach number distributions in Fig. 14(*b*) show that the spatial displacement correction results in a slight improvement in the difference between the probe-determined Mach number distribution and the undisturbed one. The complete two-step correction does not further decrease the aforementioned difference, independently of the correction coefficient used, indicating that the discrepancies in the probe-determined Mach number values are not only caused by secondary transversal velocity effects but also due to fundamental changes of the flow field around the probe that render the uniform calibration somewhat invalid.

As it can be seen in Fig. 14(*c*), the effect of the two-step correction becomes considerable on the probe-determined yaw angle distribution. The realignment of the pressure taps is not as effective in correcting the raw probe "measurements" as it is the two-step correction in which the secondary transversal velocity components are also compensated. The use of the two-step correction with the coefficient specifically recomputed for transonic flow instead of the coefficient provided by Ligrani et al. [8] further improves the yaw angle measurements. The improvement is, however, marginal, indicating that the correction coefficient reported by Ligrani et al. [8] does not lose validity at the high subsonic regimes. Nevertheless, the corrected data are not able to perfectly retrieve the undisturbed pitch-wise distribution of yaw angles, indicating that in transonic regimes, the two-step correction underpredicts the effect of the transversal velocity components.

The distributions of pitch angles are shown in Fig. 14(*d*). While the spatial displacement correction is shown to cause negligible improvements in the accuracy of the probe-determined distribution, the two-step correction helps to further decrease the difference from the undisturbed data. Nevertheless, on the pitch angle, the effect of the correction results in minor improvements.

In the following sections, the value of C used in the two-step correction is equal to the 25.1% of the probe head diameter.

3.4 Effect on the Probe Measurements in the 3D Region

3.4.1 Effect on the Flow Field Near the Shroud Endwall. Figure 15 shows contour plots of the total pressure distribution near the shroud endwall at plane 2 for the vanes-only (no probe) case and for the case with vanes and probe. For both cases, the values in the figures are normalized by the inlet total pressure, P_{01}. The total pressure values, P_{02}, corresponding to the vanes-only case are distinguished from the ones corresponding to the vanes and probe case using an asterisk. The total pressure values used for the vanes-only case were extracted directly from the simulation and represent the values obtained in an undisturbed flow field.

The values shown for the case with vanes and probe are the ones retrieved by the probe after the application of the two-step correction and include any disturbances caused by the probe to the flow field, as in the case of a typical experiment. In both cases, the characteristic low total pressure core, as a result of the upper passage vortex of the vanes, is evident. Comparing the two plots, it can be seen that the flow field retrieved by the probe is similar to the one of the vanes-only case albeit with lower total pressure values in the passage vortex and with contour lines that appear more stretched in the radial direction.

The differences between the two cases are better highlighted in the difference plot shown in Fig. 16, constructed by simple subtraction the flow fields of Figs. 15(*a*) and 15(*b*). The maximum difference between the flow field of the vanes-only case and the probe-retrieved flow field is equal to ±1.5% of the total inlet pressure. The distribution of the error plot is qualitatively different from the distributions shown in Fig. 16, indicating that the differences between the vanes-only and probe-retrieved flow fields are partly due to the aforementioned shift of the relative position of the two distributions. A second reason for the difference between the two distributions is the difference in the magnitudes of the total pressure values of the two cases.

The underlying cause of these qualitative and quantitative differences between the two flow fields can be either a fundamental change of the flow field upstream of the probe due to an influence of the probe on the upstream vane or an error in the reading of the probe due to the uniform calibration not being able to account for the flow nonuniformities in the measurement setup. These two effects could not be separated in this study, but based on the small effect of the probe on the upstream vane loading shown in Fig. 10, it is hypothesized that the primary cause is the inability

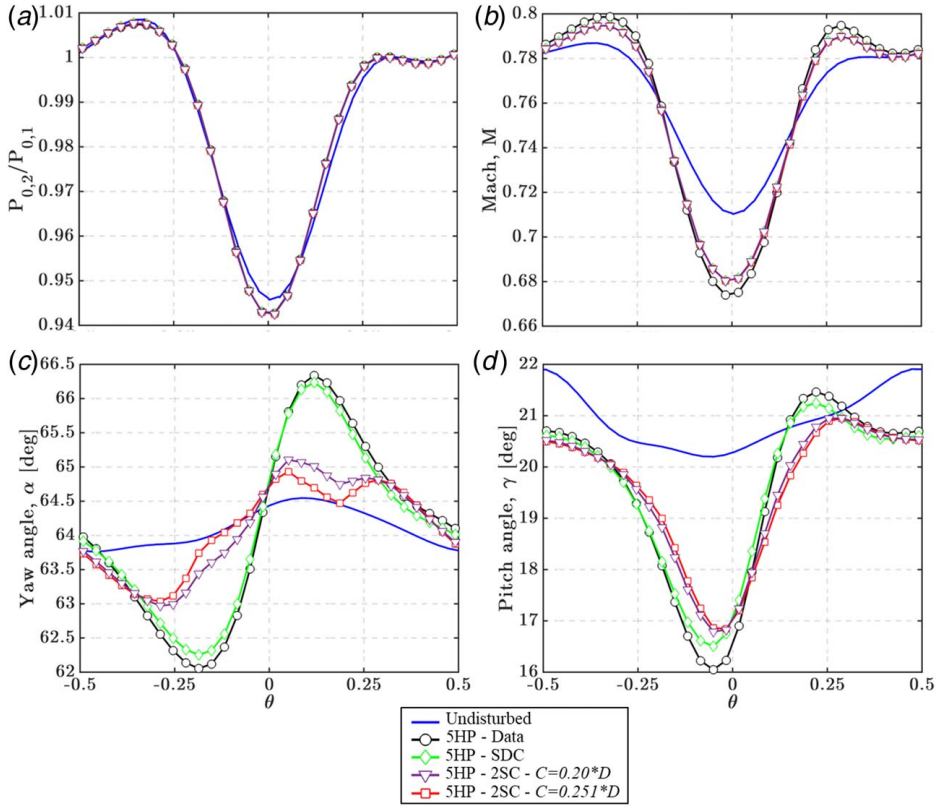

Fig. 14 Midspan pitch-wise distributions of (*a*) normalized total pressure, (*b*) Mach number, (c) yaw angle, and (*d*) pitch angle of the undisturbed flow field, measurement performed with the five-hole probe and measurement performed with the five-hole probe corrected accounting for pressure taps spatial displacements and velocity gradients

of the uniform calibration to account for the flow nonuniformities present in the measurement setup with upstream vanes.

Figure 17 shows contour plots of the Mach number distribution near the shroud endwall at plane 2, for the vanes-only (no probe) case and for the case with vanes and probe. The Mach number values for the vanes-only case are obtained directly from the simulation, and the values of the vane and probe case are the ones retrieved by the probe including the two-step correction. An asterisk is used to distinguish the Mach number values, M_2*, corresponding to the vanes-only case. A low Mach number region is observed in both figures as a result of a reduction of the flow velocity in the core of the upper passage vortex of the vanes. Compared to the vanes-only case, the probe-retrieved data show a lower Mach number in the core of the passage vortex and higher Mach number on the edges of the wake.

Figure 18 shows the differences between the Mach number distributions of the two cases. The maximum difference between the flow field of the vanes-only case and the probe-retrieved flow field is equal to 0.039 in the wake and −0.019 outside of the wake.

Figure 19 shows a contour plot of the yaw angle distribution near the shroud endwall at plane 2 (*a*) for the vanes-only case, (*b*) for the case with vanes and probe when no correction is applied, and (*c*) for the case with vanes and probe when the two-step correction is applied. As in the preceding plots, yaw angles corresponding to the vanes-only case are distinguished by an asterisk.

A region of underturning (yaw angle smaller than 64 deg of flow turning expected by vanes) stretching across much of the vane passage can be seen at about 90% span in the vanes-only case as a result of the presence of the upper passage vortex. In the same region, a noticeable difference can be seen in the case of the probe-determined flow field without correction (Fig. 19(*b*)). In this case, two adjacent regions of high and low yaw angles can be seen. Upon application of the two-step correction to the probe-determined flow field, the distribution of the yaw angle (Fig. 19(*c*)) shows a much more similar flow field to the vanes-only case, demonstrating the benefit of using this correction.

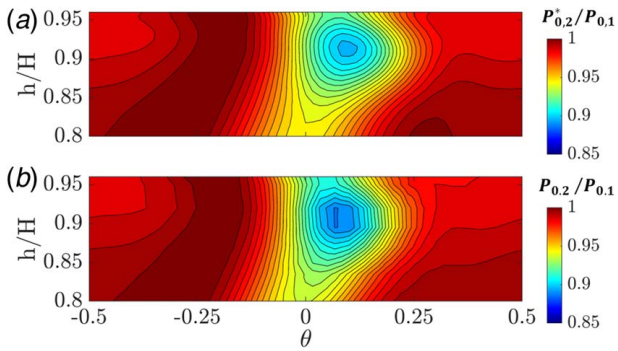

Fig. 15 Normalized total pressure distribution near the shroud endwall at plane 2: (*a*) flow field for the vanes-only case and (*b*) flow field retrieved by the probe after two-step correction

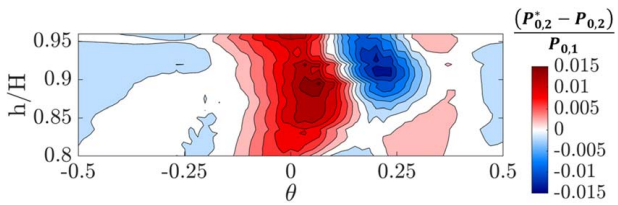

Fig. 16 Contour plot of the difference between the normalized total pressure distributions in the flow field of the vanes-only case and the flow field retrieved by the probe

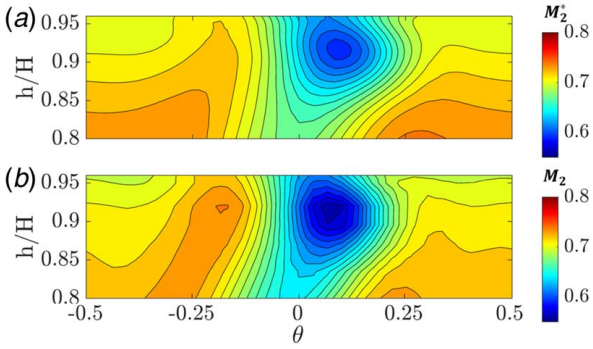

Fig. 17 Mach number distribution near the shroud endwall at plane 2: (*a*) flow field for the vanes-only case and (*b*) flow field retrieved by the probe after two-step correction

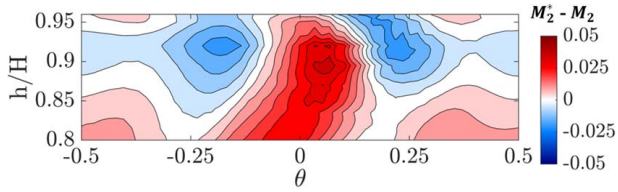

Fig. 18 Difference between Mach number contours of Fig. 17. Undisturbed case minus probe-measured data.

The benefit of using the two-step correction can be better appreciated by looking at the different plots in Fig. 20. When no correction is applied to the probe-retrieved data (Fig. 20(*a*)), the maximum yaw angle difference between the two cases is ± 5 deg. When the two-step correction is applied (Fig. 20(*b*)), the error decreases below ±1 deg from 80% to 94% of the span and below ±2.5 deg above 94% of the span, thus showing the clear benefit of using the correction. The higher error at high span is attributed to probe–endwall interaction effects that are not taken into account by the correction.

Despite not shown in this article, using the two-step correction also improves the agreement between the probe-determined pitch angle distributions and the ones retrieved in the vanes-only case.

3.4.2 Effect on the Flow Field Near the Hub Endwall. Figure 21 shows contour plots of the total pressure distribution near the hub endwall at plane 2 for the vanes-only case and for the vanes and probe case. In the latter case, the flow field is the one retrieved by the probe with the two-step correction.

A vertical region of low total pressure can be seen in the vanes-only case (Fig. 21(*a*)), corresponding to the wake of the vanes. Surprisingly no evidence of the lower passage vortex can be clearly identified in this figure likely due to the presence of a very weak vortex, which remains close to the hub endwall. As it can be seen in Fig. 21(*b*), a virtually identical flow field is retrieved by the probe with the two-step correction albeit with a slight overestimation of the total pressure values.

The differences between the two flow fields can be better visualized by looking at the difference plot in Fig. 22. The regions at which the total pressure is overestimated by the probe are found on either side of the wake. The maximum difference between the two flow fields is −1.5% of the inlet total pressure and occurs near the hub endwall on the left side of the wake (pressure side of the vane). This larger discrepancy between the two flow fields is attributed to the probe-proximity error due to a combined effect of the pre-pitch of the probe head relative to the axial direction and the curvature of the hub endwall.

Figure 23 shows contour plots of the Mach number distribution near the hub endwall at plane 2, for the vanes-only (no probe) case and for the case with vanes and probe. The data obtained for

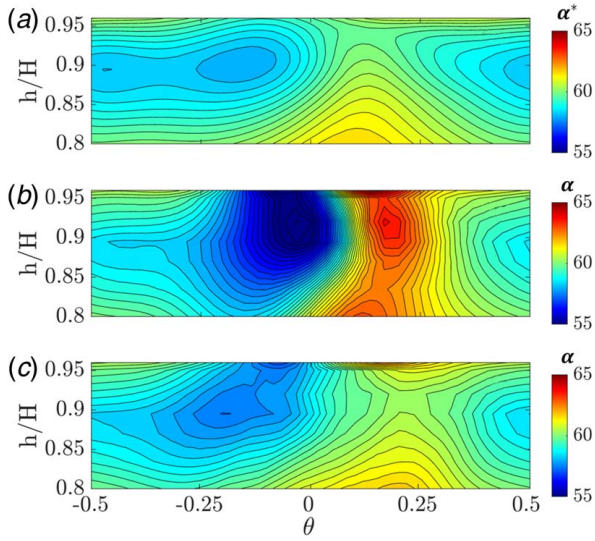

Fig. 19 Yaw angle distribution near the shroud endwall at plane 2: (*a*) flow field for the vanes-only case, (*b*) flow field retrieved by the probe, and (c) flow field retrieved by the probe after two-step correction

the vanes-only case (Fig. 23(*a*)) clearly show the low-velocity flow in the wake of the vanes. Similar to the total pressure contours, the passage vortex cannot be clearly identified. The Mach number distributions of the probe-determined flow field after the two-step correction (Fig. 23(*b*)) show an underprediction of the Mach number throughout the span-wise extend of the wake, which is larger in the region of the wake closer to the bottom endwall.

Figure 24 shows the differences between the two Mach number distributions shown in Fig. 23. The maximum difference between the vanes-only and the probe-retrieved flow fields is about 0.05 in the vertical section of the wake. As the endwall is approached, the difference increases to up to 0.8. Outside of the wake, the Mach number is overestimated by a maximum of −0.03.

Figure 25 shows the contour plots of the yaw angle distribution near the hub endwall at plane 2 for (*a*) the vanes-only case, (*b*) the case with vanes and probe when no correction is applied, and (*c*) the case with vanes and probe when the two-step correction is applied. The vanes-only case shows a region of slight underturning (yaw angle smaller than 64 deg of flow turning expected by vanes) that stretches across the pitch-wise direction. Similar to the shroud results, a large difference in the near-hub yaw angle distributions can be seen for the probe-determined flow field without correction (Fig. 25(*b*)) relative to the vanes-only case. Applying the two-step

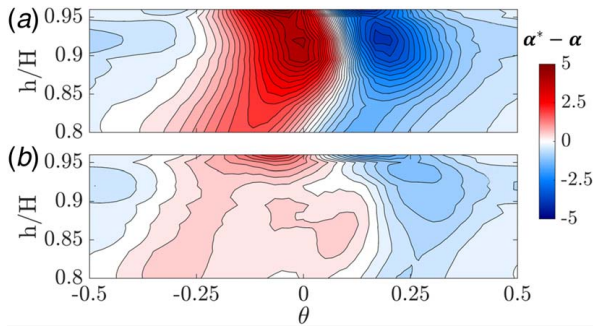

Fig. 20 Contour plot of the difference between the yaw angle distributions in the flow field of the vanes-only case and the flow field retrieved by the probe: (*a*) probe-retrieved values without correction and (*b*) probe-retrieved values including two-step correction. Plane 2 at the shroud of the flow path.

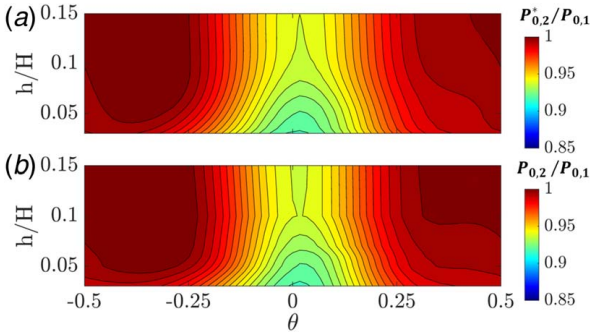

Fig. 21 Contours of normalized total pressure in plane 2 at the hub of the flow path: (*a*) value for the undisturbed case and (*b*) probe-retrieved values including two-step correction

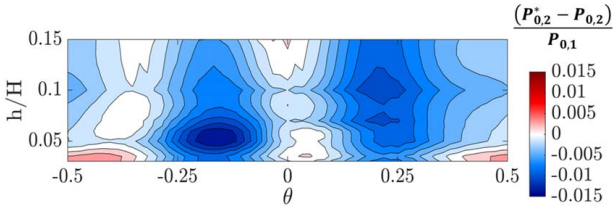

Fig. 22 Difference between the normalized total pressure contours of Fig. 21. Undisturbed case minus probe-measured data.

correction to the probe-determined flow field (Fig. 25(*c*)) results in a distribution of yaw angles, which is much closer to the undisturbed flow field of the vanes-only case.

The significance of using the two-step correction can be better appreciated when considering the differences between the probe-determined flow field with and without correction and the undisturbed flow field obtained in the vanes-only case, shown in Figs. 26(*a*) and 26(*b*), respectively.

In both figures, the maximum differences appear on either side of the wake and are larger near the endwall. When the correction is applied, a clear reduction of the differences between the probe-determined and vanes-only flow fields is achieved, from ±2.5 deg when no correction is applied to ±1 deg after the correction; an overall improvement of 1.5 deg. Near the endwall, the effect of the correction is smaller with an improvement of only 0.8 deg. As in the case of the shroud result, this smaller improvement is due to probe–endwall interaction not accounted by the correction.

3.4.3 Effect on the Pitch-Wise Averaged Distributions. Figure 27 shows the pitch-wise averaged radial distribution of (*a*) total pressure, (*b*) Mach number, (*c*) yaw, and (*d*) pitch angles.

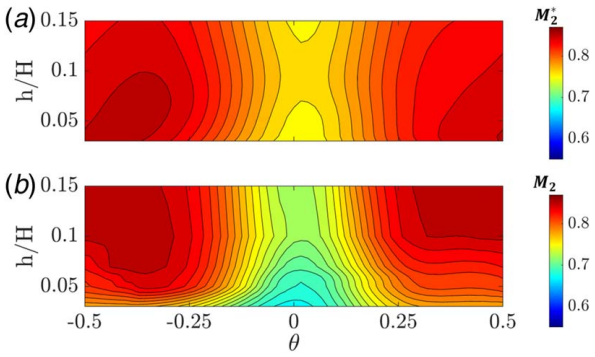

Fig. 23 Contours of Mach number value in plane 2 at the hub of the flow path: (*a*) value for the undisturbed case and (*b*) probe-retrieved values including two-step correction

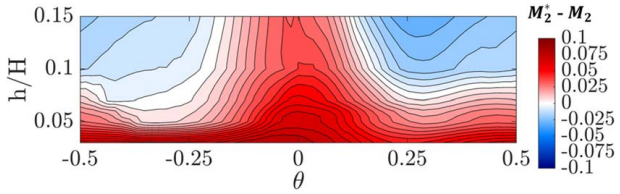

Fig. 24 Difference between Mach number contours of Fig. 23. Undisturbed case minus probe-measured data.

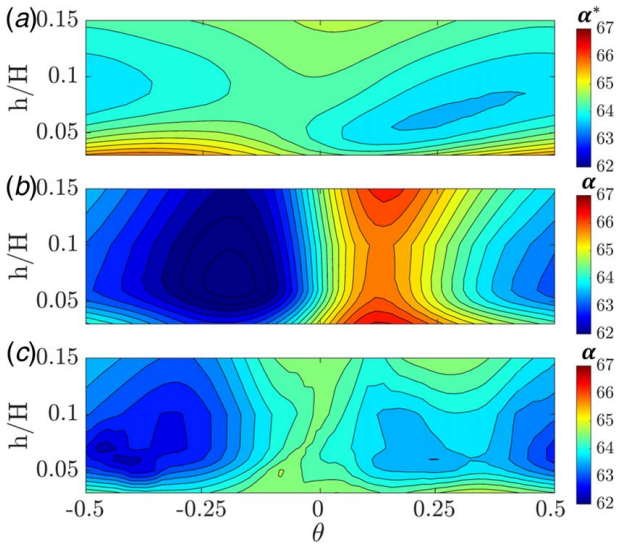

Fig. 25 Yaw angle distribution in plane 2 at the hub of the flow path: (*a*) flow field for the vanes-only case, (*b*) flow field retrieved by the probe, and (c) flow field retrieved by the probe after two-step correction

The distributions of the reference test case (blue lines), raw probe measurements (black circle symbols), and corrected probe data with the two-step approach (red squares) are also included in every plot. In general, and something applicable to all distributions, there is a perfect collapse of the data points corresponding to the uncorrected case with the ones corresponding to the corrected case. Note that this would also be the case if the correction coefficient reported by Ligrani et al. [8] was used. This indicates that the probe effect shown in the previous sections is only localized and that it does not alter the average distributions. This result could be easily expected as the transversal velocity component, which represents the most important contribution to the correction,

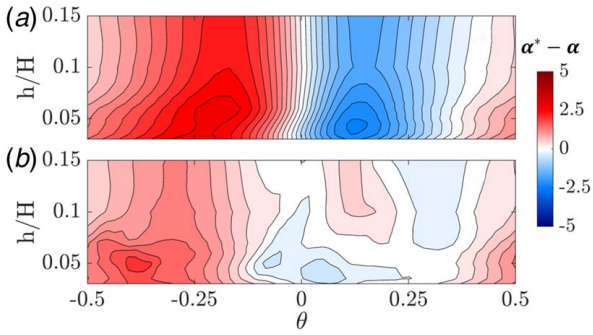

Fig. 26 Contour plot of the difference between the yaw angle distributions in the flow field of the vanes-only case and the flow field retrieved by the probe: (*a*) probe-retrieved values without correction and (*b*) probe-retrieved values including two-step correction. Plane 2 at the hub of the flow path.

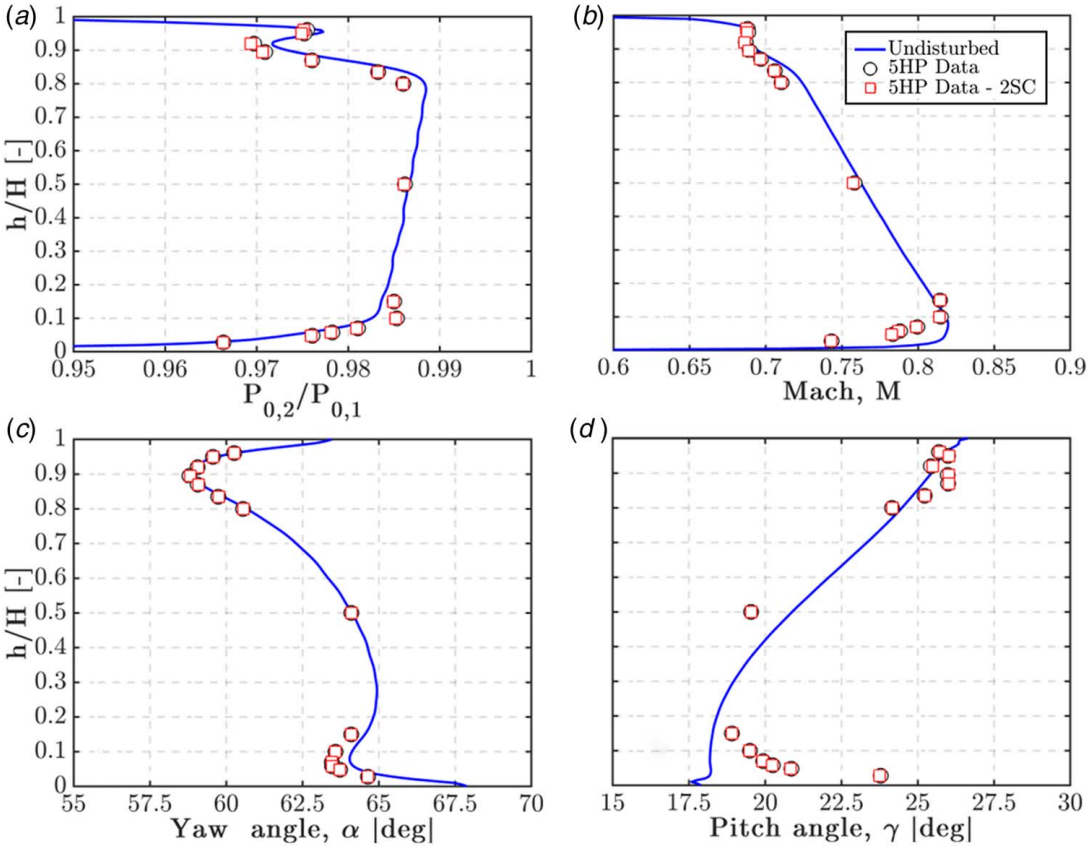

Fig. 27 Pitch-wise averaged radial distribution of (*a*) total pressure, (*b*) Mach number, (*c*) yaw angle, and (*d*) pitch angle. Comparison of undisturbed flow field, probe-measured data and probe data corrected with two-step correction.

is equal to the derivative of the periodic streamwise velocity. Its pitch-wise average is always equal to zero, thus providing null contribution to the final pitch average.

First, the total pressure distribution shown in Fig. 27(*a*) is considered. Over the entire span, the maximum difference between the probe-determined and undisturbed flow field values is ±0.25% of the total inlet pressure. The highest deviations occur in the 3D regions near the hub and shroud where the radial gradients of total pressure are stronger. The mismatch in the hub region is also due to probe–endwall interactions that induce a spurious increase in the static pressure reading of the bottom pressure tap.

Then, Fig. 27(*b*) and the radial distribution of the pitch-wise averaged Mach number are considered. At midspan and near the shroud region, the probe-determined values show good agreement with the undisturbed values with maximum errors below 0.015. At the hub, higher deviation of the probe-determined quantities is shown due to the probe–endwall interactions previously mentioned.

Then, Fig. 27(*c*) and the radial distribution of the pitch-wise averaged yaw angles are considered. As it can be seen, the probe-determined values are in good agreement with the distribution obtained for the undisturbed vanes-only case. The highest deviation is observed at the hub region, with the error in the probe-determined yaw angles below 1 deg.

Finally, Fig. 27(*d*) and the radial distribution of the circumferentially averaged pitch angles are considered. At shroud and mid-span, the deviation of the probe-determined values from the undisturbed ones is below 1.5 deg. This deviation is higher at midspan with respect to the tip due to a more conspicuous blockage effect of the probe stem. The probe stem blockage deviates the flow below the probe, thus causing the reduction of the flow angle and the value "measured" by the probe.

Close to the hub, the probe–endwall interactions induce an increase in the static pressure on the bottom tap of the probe, resulting in a strong deviation of the probe-determined values in this region.

4 Conclusion

In this study, the effects of probe–vane interactions on the flow field and probe measurements were analyzed using numerical simulations.

First, the numerical calibration was presented, for several yaw and pitch angles, and Mach numbers. Turbulence conditions were found to play a major role in the total pressure values of the flow retrieved by the probe. For this reason, the probe was calibrated at the same turbulence conditions as the ones found downstream of the vane row.

A comparison between the calibration maps obtained using the average pressure of the side holes and the ones obtained using the base pressure tap showed that the latter results in higher Mach number sensitivity, as expected, but that it also decreases the yaw angle sensitivity. The average pressure between side taps was then employed for the probe measurements.

The simulations including vane and probe showed that the probe potential field impacts the upstream vane sector causing a variation of the vane loading of five airfoils, the one immediately in front of the probe, the three lower (suction side direction) ones, and the first upper (pressure side direction) one. This impact is as a result of a static pressure change downstream of the nozzles, which alters the mass flow distribution through the passages and hence the acceleration of the flow over the vane profile.

When traversing downstream of one vane passage, the probe impact on the vane isentropic Mach number was found to depend on the probe circumferential position and to be concentrated toward the rear section of the suction side only. The highest

impact occurs when the probe is located at the upper mid-passage ($\theta = 0.5$). This impact was relatively small causing a maximum deviation from the vanes-only (no probe) case of just 0.02.

The probe-determined quantities were compared against a vanes-only test case (no probe), which was used as the reference case, representing the "undisturbed" flow field, for assessing the accuracy of the quantities determined by the probe.

At midspan, the probe-determined data showed nonnegligible differences from the undisturbed values with the highest pitch and yaw angle discrepancies found in the proximity of the strongest velocity (or total pressure) gradients. Further investigation involving stagnation point tracking showed that the artificial high circumferential variation of the yaw angle is not caused by a modification of the vane outlet flow angle but is induced by the interaction of the probe and vane.

To compensate for the effect due to velocity gradients, a two-step correction was employed. The correction coefficient used to compensate for the transversal velocity at the probe head was recomputed in the transonic regime relevant to this article and found to be 25% higher than the coefficient previously reported in the literature for subsonic regimes.

The effect of the two-step correction on the probe-determined data was evaluated in the 2D and 3D flow regions by comparison to the vanes-only flow field data extracted directly from the simulation. The total pressure distribution was accurately retrieved in the pitch-wise direction except in the wake and passage vortex regions. After correction, the Mach numbers were not precisely retrieved by the probe, suggesting that inaccuracies cannot be corrected by only accounting for the secondary transversal velocity component that arises on the probe head but should be compensated on the pressure reading of the taps. The correction was shown to be very effective on the "measured" yaw angles on both the 2D and 3D regions, reducing the difference between vanes-only and probe-determined data below 1 deg. It was also shown that the new correction coefficient recomputed for transonic Mach numbers further improves the yaw angle measurements. The improvement was, however, marginal, indicating that the correction coefficient previously reported in the literature by Ligrani et al. [8] can also be used for high subsonic regimes. The use of the two-step correction stands as a powerful tool to drastically reduce the errors on the measured angles, and it is recommended to be employed in experimental campaigns using multi-hole probe measurements. However, an error remains that is thought to be due to underprediction of the transversal velocity component effect in the transonic regime. To mitigate this residual error, reducing the size of the probe to as small as possible is recommended.

Finally, the effect on the pitch-wise averaged measured quantities was evaluated. The highest variation between probe-determined data and undisturbed values was found where radial gradients of total pressure are stronger. Furthermore, the two-step correction was shown to have an almost negligible impact on the pitch-wise averaged quantities, with the data including the correction being identical to the uncorrected raw probe data.

Acknowledgment

The authors gratefully acknowledge funding of the SPLEEN project by the Clean Sky 2 Joint Undertaking under the European Union's Horizon 2020 research and innovation program (Grant No. 820883).

Conflict of Interest

There are no conflicts of interest.

Data Availability Statement

The datasets generated and supporting the findings of this article are obtainable from the corresponding author upon reasonable request.

Nomenclature

d = distance between taps/diameter
M = Mach number
C = correction coefficient
D = diameter
K = calibration coefficient
L = length
P = pressure
R = specific gas constant
C_{ax} = vane axial chord
P_{ave} = side holes average static pressure
P_{BP} = pressure reading from base pressure tap

Greek Symbols

α = yaw angle
α_{cone} = probe cone angle
γ = pitch angle/heat capacity ratio
θ = nondimensional vane pitch

Subscripts

0 = total quantity
1 = inlet
2 = measurement plane
C = central tap
D = down tap
h = horizontal
in = inner
L = left tap
max = maximum value
out = outer
R = right tap
side = side holes
tot = total pressure coefficient
u = uncorrected
U = up hole
v = vertical

Appendix: Calibration of the Correction Coefficient C

The determination of the correction coefficient, C, was accomplished using the probe calibration setup and imposing a nonuniform inlet total pressure distribution in the pitch-wise direction to introduce a wake upstream of the probe. The width and depth of the wake have been selected to replicate the wake from the test. Simulations have been performed with inlet yaw and pitch angles equal to zero. The outlet static pressure have been imposed accordingly to the desired flow Mach number.

Simulations were run at three Mach numbers, M = 0.7, 0.8, and 0.9. Lower freestream Mach numbers have not been tested to ensure that the probe measurements stay within the calibration range.

To replicate the probe traversing, five RANS simulations were performed for every of the tested Mach numbers, varying the inlet wake position relatively to the probe head position.

First, the local displacement of the side taps on the probe head with respect to the central tap was corrected. Second, the measured flow velocity was used to compute the gradient of axial velocity in the tangential direction. The correction factor is obtained from the following formula:

$$C = \frac{V_x - V_{xu}}{\frac{dVz}{dx} D}$$

where V_{xu} is the uncorrected components of tangential velocity, V_x is the corrected component of tangential velocity and equals to zero as no inlet flow angle is imposed at the inlet of the domain, V_z is the axial velocity component, and D is the probe diameter.

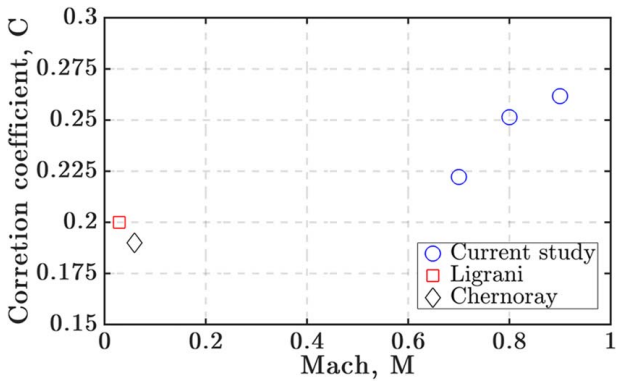

Fig. 28 Effect of Mach number on the value of the correction coefficient

Figure 28 shows a plot of correction factors obtained in the current study against data of Ligrani et al. [8] and Chernoray and Hjärne [9]. This figure shows that the Mach number has an influence on the value of the correction coefficient.

References

[1] Wyler, J. S., 1975, "Probe Blockage Effects in Free Jets and Closed Tunnels," J. Eng. Power, **97**(4), pp. 509–514.

[2] Truckenmüller, F., and Stetter, H., 1996, "Measurement Errors With Pneumatic Probes Behind Guide Vanes in Transonic Flow-Fields," 13th Symposium on Measuring Techniques for Transonic and Supersonic Flow in Cascades and Turbomachines, Zürich, Switzerland, Sept. 5–6.

[3] Boerner, M., Bitter, M., and Niehuis, R., 2018, "On the Challenge of Five-Hole-Probe Measurements at High Subsonic Mach Numbers in the Wake of Transonic Turbine Cascades," J. Glob. Power Propuls. Soc., **2**, pp. 453–464.

[4] Aschenbruck, J., Hauptmann, T., and Seume, J. R., 2015, "Influence of a Multi-Hole Pressure Probe on the Flow Field in Axial-Turbines," 11th European Conference on Turbomachinery Fluid Dynamics & Thermodynamics, Madrid, Spain, Mar. 23–27.

[5] Sanders, C., Terstegen, M., Hölle, M., Jeschke, P., Schönenborn, H., and Fröbel, T., 2017, "Numerical Studies on the Intrusive Influence of a Five-Hole Pressure Probe in a High-Speed Axial Compressor," Proceedings of the ASME Turbo Expo 2017: Turbomachinery Technical Conference and Exposition. Volume 2A: Turbomachinery, ASME, Charlotte, NC, June 26–30, p. V02AT39A009.

[6] Hoenen, H. T., Kunte, R., Waniczek, P., and Jeschke, P., 2012, "Measuring Failures and Correction Methods for Pneumatic Multi-Hole Probes," Proceedings of the ASME Turbo Expo 2012: Turbine Technical Conference and Exposition. Volume 1: Aircraft Engine; Ceramics; Coal, Biomass and Alternative Fuels; Controls, Diagnostics and Instrumentation, ASME, Copenhagen, Denmark, June 11–15, pp. 721–729.

[7] Clark, C. J., and Grimshaw, S. D., 2019, "A Pneumatic Probe for Measuring Spatial Derivatives of Stagnation Pressure," Proceedings of the ASME Turbo Expo 2019: Turbomachinery Technical Conference and Exposition. Volume 6: Ceramics; Controls, Diagnostics, and Instrumentation; Education; Manufacturing Materials and Metallurgy, ASME, Phoenix, AZ, June 17–21, p. V006T05A024.

[8] Ligrani, P. M., Singer, B. A., and Baun, L. R., 1989, "Spatial Resolution and Downwash Velocity Corrections for Multiple-Hole Pressure Probes in Complex Flows," Exp. Fluids, **7**(6), pp. 424–426.

[9] Chernoray, V., and Hjärne, J., 2008, "Improving the Accuracy of Multihole Probe Measurements in Velocity Gradients," Proceedings of the ASME Turbo Expo 2008: Power for Land, Sea, and Air. Volume 2: Controls, Diagnostics and Instrumentation; Cycle Innovations; Electric Power, ASME, Berlin, Germany, June 9–13, pp. 125–134.

[10] Boerner, M., and Niehuis, R., 2018, "Development of the Additive Manufactured Miniaturized Wedge Probe Optimized for 2d Transonic Wake Flow Measurements," 24th Biannual Symposium on Measuring Techniques in Turbomachinery, Prague, Czech Republic, Aug. 30–31.

[11] Passmann, M., aus der Wiesche, S., and Joos, F., 2021, "Numerical Calibration of Three-Dimensional Printed Five-Hole Probes for the Transonic Flow Regime," ASME J. Fluids Eng., **143**(5), p. 051501.

[12] Schäffer, C., Speck, K., and Gümmer, V., 2021, "Numerical Calibration and Investigation of the Influence of Reynolds Number on Measurements With Five-Hole Probes in Compressible Flows," Proceedings of the ASME Turbo Expo 2021: Turbomachinery Technical Conference and Exposition. Volume 4: Controls, Diagnostics, and Instrumentation; Cycle Innovations; Cycle Innovations: Energy Storage; Education; Electric Power, ASME, Virtual, June 7–11, p. V004T05A002.

[13] Menter, F. R., 1994, "Two-Equation Eddy-Viscosity Turbulence Models for Engineering Applications," AIAA J., **32**(8), pp. 1598–1605.

[14] Yasa, T., and Paniagua, G., 2012, "Robust Procedure for Multi-Hole Probe Data Processing," Flow Meas. Instrum., **26**, pp. 46–54.

[15] Hall, B. F., and Povey, T., 2017, "The Oxford Probe: An Open Access Five-Hole Probe for Aerodynamic Measurements," Meas. Sci. Technol., **28**(3), p. 035004.

[16] Issa, R. I., 1995, "Rise of Total Pressure in Frictional Flow," AIAA J., **33**(4), pp. 772–774.

[17] Norris, S. E., 2011, "The Effect of Nonuniform Viscosity on Stagnation Point Pressure," ASME J. Fluids Eng., **133**(4), p. 044501.

[18] Williams, D. M., Kamenetskiy, D. S., and Spalart, P. R., 2016, "On Stagnation Pressure Increases in Calorically Perfect, Ideal Gases," Int. J. Heat Fluid Flow, **58**, pp. 40–53.

[19] Main, A. J., Day, C. R. B., Lock, G. D., and Oldfield, M. L. G., 1996, "Calibration of a Four-Hole Pyramid Probe and Area Traverse Measurements in a Short-Duration Transonic Turbine Cascade Tunnel," Exp. Fluids, **21**(4), pp. 302–311.

[20] He, L., and Ning, W., 1998, "Efficient Approach for Analysis of Unsteady Viscous Flows in Turbomachines," AIAA J., **36**(11), pp. 2005–2012.

[21] Green, B. R., Mathison, R. M., and Dunn, M. G., 2014, "Comparison of Harmonic and Time Marching Unsteady Computational Fluid Dynamics Solutions With Measurements for a Single-Stage High-Pressure Turbine," ASME J. Turbomach., **136**(1), p. 011005.